Available online at www.sciencedirect.com
SCIENCE DIRECT®
Polymer 45 (2004) 1391–1399
polymer
www.elsevier.com/locate/polymer

Molecular response of a glassy polymer to active deformation

Franco M. Capaldi[a], Mary C. Boyce[a], Gregory C. Rutledge[b,*]

[a]Department of Mechanical Engineering, Massachusetts Institute of Technology, 77 Massachusetts Avenue, Cambridge, MA 02139, USA
[b]Department of Chemical Engineering, Massachusetts Institute of Technology, 77 Massachusetts Avenue, Cambridge, MA 02139, USA

Received 6 March 2003; received in revised form 28 July 2003; accepted 31 July 2003

Abstract

The behavior of a glassy polyethylene-like polymer undergoing active compressive deformation was investigated via molecular dynamics simulation. Several important features can be identified within the stress–strain response of the system. Namely, the system deforms elastically, yields, softens, and then at large strains exhibits strain hardening. Simulations reveal that the actively deforming polymer exhibits several distinct characteristics at the molecular scale. Active deformation is found to significantly increase the transition rate between different dihedral angle states as well as promote the propagation of dihedral angle flips along the chain. When deformation is stopped, the transition rates decrease and propagation of these transitions along the chain is once again hindered. Below the glass transition temperature, transitions are heterogeneously distributed within the system. However, a local density-transition rate correlation study shows that this transitional heterogeneity is not attributable to heterogeneity in the local density. Instead, the high local transition rates must be caused by stresses propagated along the chain backbone as indicated by changes in neighbor correlations with stress. The yield stress is determined as a function of strain rate between strain rates of 10^8 s^{-1} and 5×10^{10} s^{-1}. The activation volume within the context of the Eyring model is calculated to be 0.21 nm^3 for this system.

Keywords: Plasticity; Glass deformation; Molecular dynamics

1. Introduction

The molecular origins of plastic deformation within glassy amorphous polymers are not well understood. The lack of long range order within these systems precludes the use of theories based on dislocation motion that have been so successful within crystalline solids. Instead, several theoretical models build on the notion that small localized transformations occur within the material in response to an applied stress [1–3]. The Eyring model [1] postulates that the energy barrier to these localized transformations is modified by the application of stress. This model reveals nothing about the underlying molecular process and fails to describe the behavior over wide ranges of temperature and strain rate [2]. The Robertson theory [2] assumes that the applied stress alters the energy level associated with the rotational isomeric state of a dihedral angle along the chain. The bias in favor of the *cis* over the *trans* state creates regions in the material that have *cis* content similar to that found in the liquid state. The Argon model considers the barrier to be due to the resistance to molecular segmental rotation posed by intramolecular and intermolecular interactions of the chain with the surrounding material [3].

More recently, computer simulations have been used to elicit the molecular details of plastic flow within polymeric systems. Molecular mechanics simulations of chemically detailed models of polypropylene [4,5] and polycarbonate [6] undergoing quasi-static deformation revealed discrete plastic events with transformation shear strains on the order of 0.017 within simulation cells with side length of 1.815 and 3.396 nm. Subsequent normal mode analysis of polyethylene-like chains undergoing similar quasi-static deformations suggested that these discrete plastic events could be attributed to the changing character of the potential energy landscape [7,8]. By its nature, the quasi-static deformation realized by molecular mechanics calculations give rise to 'catastrophic' rearrangements of the material once a barrier in the energy landscape is crossed (or removed). The simulations of simple polyethylene-like chains using molecular dynamics [9,10] and Monte Carlo [11] revealed the ability of computer simulation to

* Corresponding author. Tel.: +1-617-253-0171; fax: +1-617-258-0546.
E-mail address: rutledge@mit.edu (G.C. Rutledge).

0032-3861/$ - see front matter © 2003 Elsevier Ltd. All rights reserved.
doi:10.1016/j.polymer.2003.07.011

reproduce the qualitative behavior of glassy polymers under the influence of thermal motion. Molecular dynamics simulations have recently been used to investigate the multiaxial yield conditions for semiflexible glassy polymers [12].

Experimental investigation of these molecular mechanisms is complicated by the difficulty of collecting conformation-specific data during active deformation. Only recently have experiments begun to reveal transient features of the molecular response during the active deformation of polymers. NMR experiments on deuterated semicrystalline Nylon 6 have demonstrated stress-induced mobility within the amorphous regions [13–15]. Case II diffusion experiments on glassy poly(ether imide) have demonstrated that the diffusional uptake of the actively plastically deforming polymer below T_g is nearly identical to that at T_g in the absence of plastic deformation [16], demonstrating a dilation of the polymeric material induced by plastic flow. It has been observed that similar shear-induced dilation in metallic glasses leads to crystallization near the tip of a nano-indenter [17].

In the current work, the relation between the mobility of the dihedral angles along the polymer chain and the deformation and yield of the system is examined. For this purpose, non-equilibrium molecular dynamics simulations (NEMD) of a polyethylene-like chain were carried out at a variety of temperatures and strain rates. A brief report of selected results from this work that clearly demonstrate the appearance of stress-induced mobility has been published elsewhere [18].

2. Simulation details

A united atom model was used to represent the molecular structure of polyethylene. The functional form and parameters of the force field are provided in Table 1. The parameters were fit to those of Paul et al. [19] with the exception that stiff springs were used to represent the bonds in this study whereas rigid bonds were used in the force field of Paul et al. A similar force field was used to study crystallization of eicosane, with good results [20]. The non-bonded interactions are truncated at a distance of 10 Å and are not calculated for beads that are separated by fewer than four bonds.

A velocity Verlet algorithm [21] with an integration time step of 1 fs was used. The pressure within the simulation cell was maintained at the target value by rescaling the volume of the cell using the approach of Berendsen et al. [22] with a barostat constant of 1 ps. The Nose–Hoover thermostat [23,24] with a kinetic mass of 2.8×10^{-14} J s^2 was used to maintain a constant temperature.

Dihedral angle transitions between the trans and the gauche states were monitored following the procedure of Han et al. [25]. The dihedral angle potential exhibits three minima labeled the '*gauche* plus' ($g+$), '*trans*' (t), and '*gauche* minus' ($g-$) states, with energy minima located at 60, 180, and 300°, respectively. A dihedral angle is given a label corresponding to a particular dihedral state when it obtains a value within 10 degrees of the minimum energy value of that state. A transition is counted when the label of a dihedral angle changes, i.e. it obtains a value within 10 degrees of a different minimum energy value.

The initial structures were generated by growing polymer chains with fixed bond lengths, fixed bond angles, and random dihedral angles within the simulation cell. The interaction potential was then applied and the system was equilibrated using a Metropolis Monte Carlo algorithm [26] with single atom displacement moves for 5×10^3 steps per atom at fixed volume. Each system was then equilibrated at constant particle number, pressure, and temperature (NPT) for 200 ps. For the system with 250 beads per chain and a total of 40,000 beads used in the deformation studies, the equilibrated cell at 200 K and one atmosphere of pressure was 10.1 nm on a side.

Deformation was simulated by controlling displacement of the x dimension of the simulation cell and allowing the y and z dimensions of the cell to fluctuate according to the barostat, corresponding to the $NL_x\sigma_y\sigma_z T$ ensemble.

3. Results

3.1. Glass transition

The deformation studies were conducted at temperatures

Table 1
Functional form and parameters for force field model of united atom polyethylene

Interaction	Form	Parameters
Bond	$E = \frac{1}{2}k_b(l - l_{eq})^2$	$k_b = 2000$ kJ/mol Å^2, $l_{eq} = 1.53$ Å^2
Angle	$E = \frac{1}{2}k_\theta(\cos(\theta) - \cos(\theta_{eq}))^2$	$k_\theta = 510$ kJ/mol, $\theta_{eq} = 110°$
Torsional	$E = \frac{1}{2}\sum_{n=0}^{3} k_n \cos^n(\phi)$	$k_0 = 14.477$ kJ/mol, $k_1 = -37.594$ kJ/mol, $k_2 = 6.493$ kJ/mol, $k_3 = 58.499$ kJ/mol
Non-bonded	$E = \begin{cases} 4\epsilon\{(\frac{\sigma}{r})^{12} - (\frac{\sigma}{r})^6\} & r < r_c \\ 0 & r \geq r_c \end{cases}$	$\epsilon = 0.468$ kJ/mol, $\sigma = 4.01$ Å, $r_c = 10.0$ Å

below the glass transition temperature to ensure that a glassy response is obtained from the material model. The glass transition temperature was identified by the change in the slope of the specific volume versus temperature curve [25,27–30]. A simulation cell containing four chains with 1000 beads each was equilibrated at 500 K for 200 ps. The density of the system was monitored while cooling step-wise at an effective rate of 12.5×10^{10} K/s with the external pressure set to 1 atm, Fig. 1. The resulting transition temperature was found to be 280 ± 32 K. This falls within the range of transition temperatures, between 200 and 300 K, found for various potential models of polyethylene [25,29,30] at similar cooling rates. The experimentally reported glass transition temperature of polyethylene is 250 K [31].

3.2. Deformation and transition rates

Systems were deformed in compression at several true strain rates between 10^8 and 10^{11} s^{-1} and at 100 and 200 K. Both of these temperatures are well below the glass transition temperature of 280 K determined for this model system. Deformation along the axial direction was controlled by scaling the size of the simulation cell and positions of the atoms at each time step. The external pressure was set to one atmosphere and fluctuation of the lateral dimensions was regulated by the barostat.

The simulated mechanical and torsional responses are shown in Fig. 2 for three constant true compressive strain rates, 5×10^9, 1×10^{10}, and 5×10^{10} s^{-1}. The mechanical response is qualitatively similar to that obtained experimentally at strain rates ranging from 10^{-3} to 10^4 per second [32–34]. The stress–strain behavior initially exhibits a linear elastic response followed by a non-linear transition to yield at a compressive strain of about 0.15. Upon yielding, the material experiences strain softening followed by a stress plateau at a strain of about 0.30. The material density decreases during softening, but remains constant during the stress plateau, for strains beyond about 0.4, as shown in Fig. 3. Strain hardening then ensues at strains greater than 0.5. The Poisson ratio was calculated to be 0.35 by determining the lateral contraction of the simulation cell at a compressive strain of 0.05. From the slope of the stress–strain curve at low strain, the elastic modulus was found to be approximately 2.5 GPa. Note that the modulus value is consistent with the modulus values of glassy polymers; the yield stress value is much higher than typical values and thus the strain at yield is larger than that observed in most glassy polymers (approximately 0.15 as opposed to approximately 0.07). This will be commented upon further in the paper.

During deformation, there is a significant monotonic increase in the dihedral angle transition rate with strain, shown in Fig. 2, indicating significant torsional activity during deformation. The transition rate continues to increase

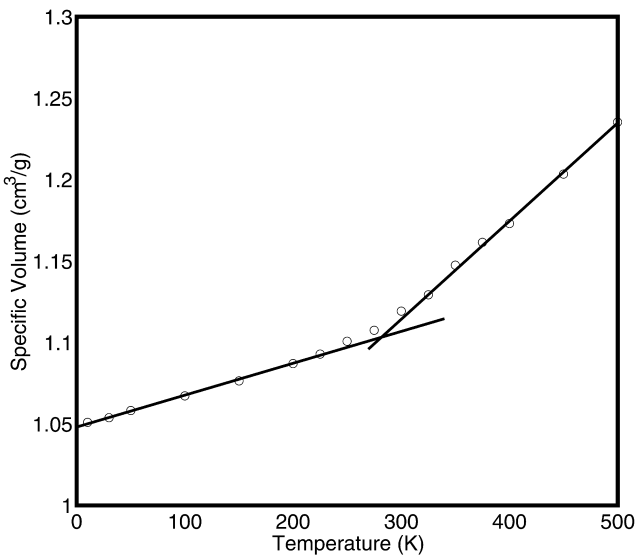

Fig. 1. Specific volume as a function of temperature during quenching.

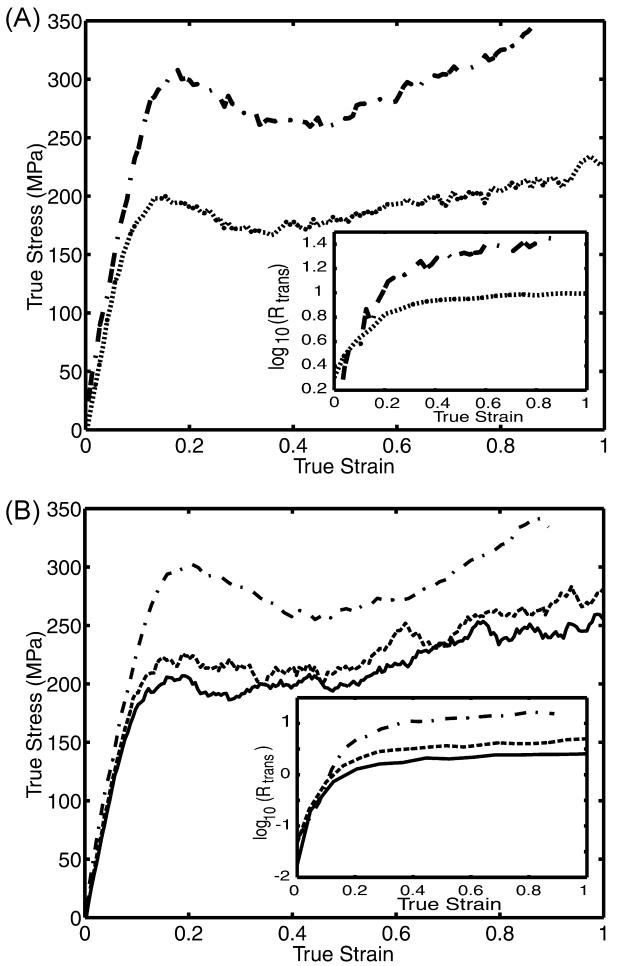

Fig. 2. Compressive true stress versus true strain at (A) 100 K and (B) 200 K and deformed at constant true strain rates of 5×10^9 s^{-1} (solid line), 1×10^{10} s^{-1} (dashed line), 5×10^{10} s^{-1} (dot dash line). The inset graph displays the logarithm of the transition rate per bond per nanosecond, R_{trans}, as a function of true strain.

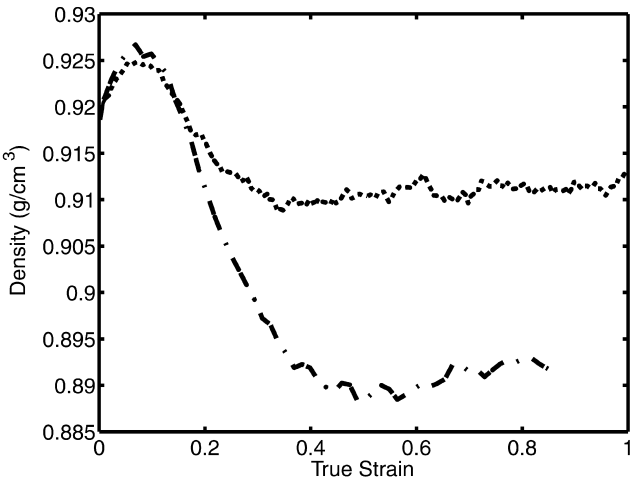

Fig. 3. Density versus true strain at 200 K for a true strain of $1 \times 10^{10}\ s^{-1}$ (dashed line), $5 \times 10^{10}\ s^{-1}$ (dot dash line).

with strain, although more slowly, as the structure yields and softens. The dependence of transition rates on deformation rate is minor during elastic deformation, but is significant following yield. Although there is significant torsional activity during deformation, the fraction of dihedral angles in the trans configuration remains constant prior to and just after yield and later increases only as strain hardening ensues, as shown in Fig. 4. This agrees well with NMR data from Utz et al. [35] which indicate that the distribution of dihedral angle conformations does not change significantly after deformation up to strains as large as 0.68.

To explore the role of volume dilation on the observed behavior, a cell was deformed axially in compression at a strain rate of 1×10^{10} per second at constant volume, as opposed to the studies described above where the lateral dimensions were free to expand or contract to maintain constant lateral stress. The simulation displayed the same

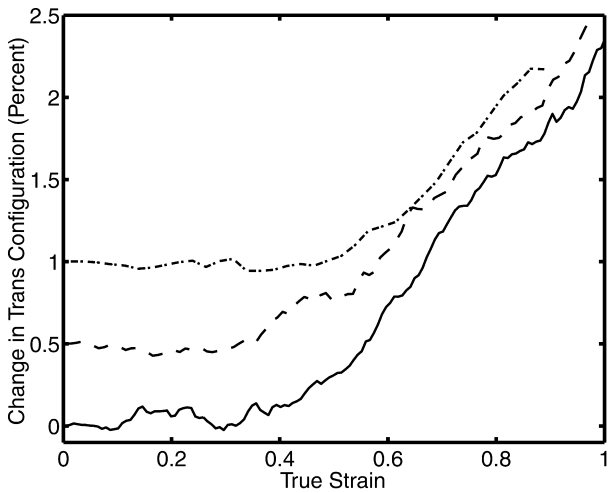

Fig. 4. Percent change of dihedral angles in the *trans* configuration at 100 K for $5 \times 10^{9}\ s^{-1}$ (solid line), $1 \times 10^{10}\ s^{-1}$ (dashed line), $5 \times 10^{10}\ s^{-1}$ (dot dash line). Each curve is displaced vertically by 0.5.

characteristic increase in the transition rate, Fig. 5, as was observed for the unconstrained systems. However, strain softening was completely suppressed in this case, implying that strain softening correlates with dilation.

In order to mimic the recent NMR experiments of Loo et al. [15], stress relaxation simulations were conducted; these results are shown in Fig. 6. The cell was deformed in uniaxial compression at a constant true strain rate of $1 \times 10^{10}\ s^{-1}$ to a strain of 0.4, relaxed with the axial dimension held fixed, deformed again in compression at a constant true strain rate of $1 \times 10^{10}\ s^{-1}$, and relaxed again with the axial dimension fixed. The transition rates are found to increase steadily with deformation and to decay abruptly as the sample is allowed to relax at constant strain. During the second deformation cycle, a higher yield stress and a correspondingly higher transition rate are observed, followed once again by a decay in both the stress and transition rate as the sample relaxes with fixed axial dimension.

As found in the compression simulations of Fig. 3, the system density increases during elastic deformation and the system dilates following yield, as shown in Fig. 7. The density returns to its original value of approximately 0.921 g/cm^3 during the first relaxation segment and then to a value higher than the original density during the second relaxation segment, which is due to additional orientation of the chains introduced through deformation.

3.3. Correlation of local density and transitions

To test the hypothesis that the occurrence of transitions along the chain correlates with the local density, the simulation cell from a non-deforming simulation was divided into subcells. Three different sizes of subcells, 0.502, 0.628, and 1.678 nm on a side, were used. Each atom, *i*, was approximated as a cube with side length of

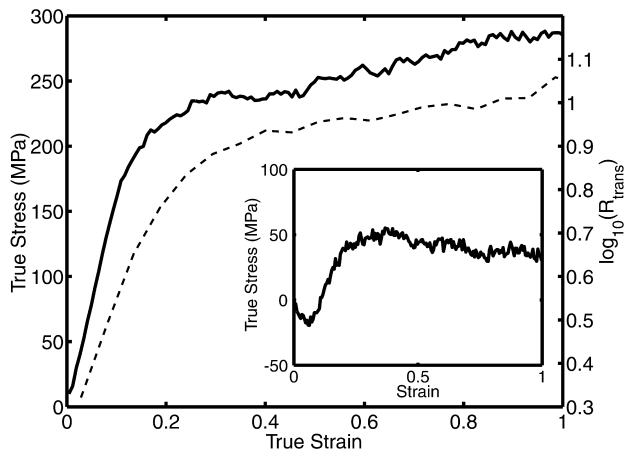

Fig. 5. Compressive true stress and logarithm of the transition rate per bond per nanosecond, R_{trans}, (dashed line) versus true strain at 100 K and deformed at constant true strain rates of $1 \times 10^{10}\ s^{-1}$. The inset graph displays the average lateral stress as a function of true strain.

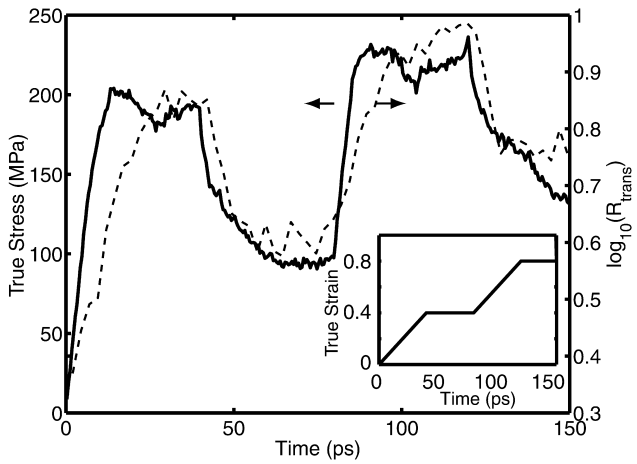

Fig. 6. Compressive true stress (solid line) and logarithm of the transition rate per bond per nanosecond, R_{trans}, (dashed line) versus time for a system at 200 K. The inset displays the true strain as a function of time.

$\sigma = 0.401$ nm and the fraction of cube i falling within subcell k at time t, $f_{ik}(t)$, was calculated. Since the bond length is 0.153 nm, many of these boxes overlap. This leads to a small shift in the computed local density towards higher values, but otherwise does not affect the correlation analysis that follows. The density within subcell k at time t, d_k, is given by

$$d_k = \frac{\int_t^{t+\Delta t} \sum_i m_i f_{ik}(t) \mathrm{d}t}{V_{\mathrm{subcell}} \Delta t}$$

where m_i is the mass of atom i, Δt is 0.5 ps, and V_{subcell} is the volume of the subcell.

The transition rate is calculated for each of the dihedral angles within the system and the value is evenly divided among the four atoms that define the dihedral angle. In this way a transition rate at time t, $R_i(t)$, can be associated with a single atom. The transition rate for a particular cell, R_k, is then given by

$$R_k = \frac{\int_t^{t+\Delta t} \sum_i R_i(t) f_{ik}(t) \mathrm{d}t}{\int_t^{t+\Delta t} \sum_i f_{ik}(t) \mathrm{d}t}$$

Figs. 8 and 9 display the log of the local transition rate, $\log_{10}(R_k)$, versus the local density, d_k, for each of the subcells in a non-deforming and a deforming cell, respectively. From this we conclude that the transition rate is statistically insensitive to local density over most of the relevant range of density. This suggests that the transitions in the non-deforming and the actively deforming system are not influenced significantly by the surrounding molecules. To confirm this unexpected result, an analysis of the transition rates in a system at 200 K under theta conditions was conducted by turning off all non-bonded interactions.

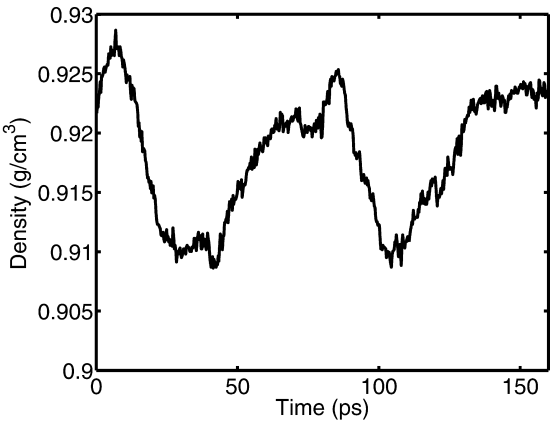

Fig. 7. Density versus time for a system at 200 K with the strain history shown in the inset of Fig. 6.

The resulting transition rate of 2.31 transitions per nanosecond per bond was found to be similar to the results of 2.20 transitions per nanosecond per bond for a simulation at 200 K with full non-bonded interactions. This difference of less than 5% suggests that, at least for polyethylene, the dihedral angle transition rate is not affected by the local density of the surrounding molecules. However, other polymer architectures may differ in this regard; for example, the energy barrier for phenyl ring motion in glassy polystyrene has been shown elsewhere to be sensitive to local packing density [36,37].

3.4. Neighbor correlations

A correlation between transitions along single chains has been observed in many studies [30,38–40]. This intramolecular correlation is assessed by determining the probability that a dihedral angle transition at a particular site along the chain is followed by another transition at a site separated by j bonds from the original site. After a transition occurs at a given site, i, the next transition to occur within 10 or fewer bonds of the first is noted. The number of bonds separating each of these pairs is recorded and the resulting probability distribution for the separation is given in Fig. 10 as a function of temperature.

At temperatures above T_g, the intramolecular dihedral transition correlation is essentially uniform, implying that transitions are uncorrelated events. As the temperature is lowered within a system of chains, dihedral transitions become heterogeneously distributed. The self correlation, $P(i \pm 0)$, of transitions increases dramatically [39,41,42]. This is consistent with the notion that torsional dynamics below the glass transition temperature are ‘caged in’ with heterogeneous local environments. However, in the absence of any significant correlation between local density and transition rate, it seems likely that the origin of heterogeneity is intramolecular, rather than intermolecular, in origin.

During deformation the nature of the intramolecular dihedral transition correlation changes. This correlation

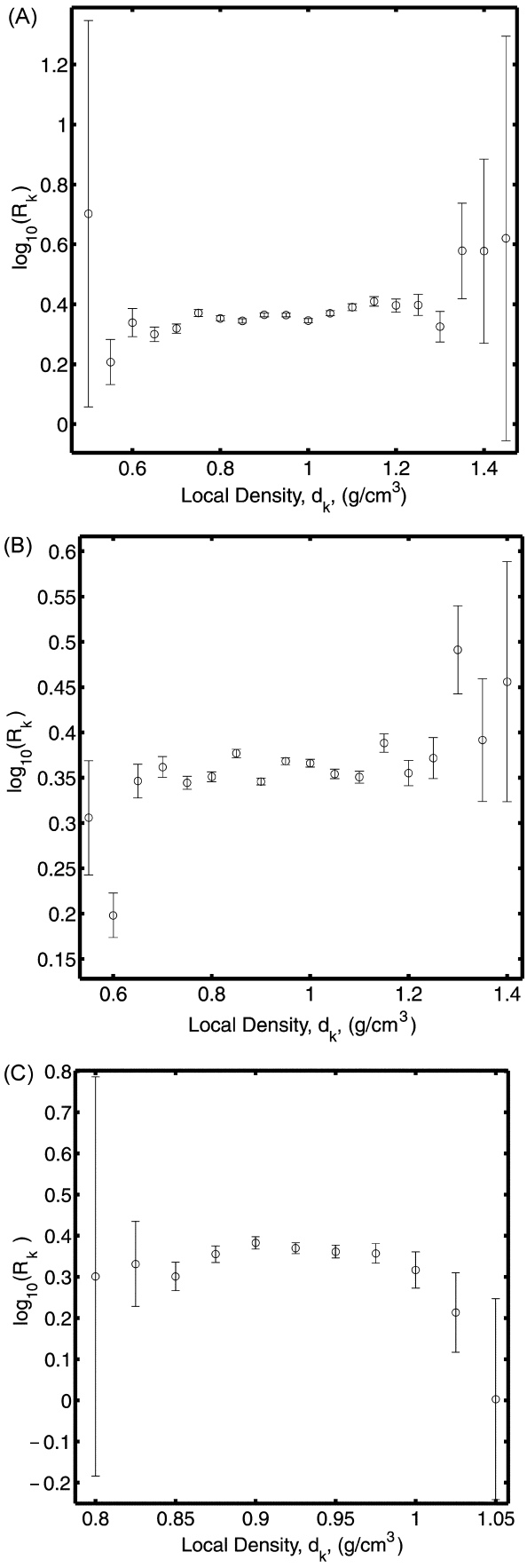

Fig. 8. The log of the local transition rate per bond per nanosecond, R_k, versus local density in a non-deforming cell at 200 K for bin width of (A) 5.02 Å, (B) 6.28 Å, and (C) 16.78 Å. The homogenization suggested by the different abscissa scales in these plots is simply a consequence of averaging over different subcell volumes. The average density is 0.921 g/cm^3 and the average log of the transition rate per bond per nanosecond is 0.36.

function was calculated for transitions occurring during active deformation after the system had reached a compressive strain, ϵ, of 0.3 for two different strain rates at 200 K; these results are shown in Fig. 11. The self correlation which is extremely strong within the non-deforming system decreases significantly during active deformation, even for systems below their T_g. The distribution for the deforming system in Fig. 11 resembles most closely the distribution at 300 K in Fig. 10.

Fig. 12 displays the neighbor correlation for a system subjected to periods of active deformation and relaxation as shown within the inset. The neighbor correlation is calculated over different intervals in time during the simulation and compared to a correlation for the sample prior to deformation. The self-correlation decreases sharply during active deformation but increases during relaxation.

3.5. Activation volume

By measuring the yield stress as a function of strain rate, the activation volume in the context of the Eyring model may be determined. The Eyring model assumes the deformation process has associated with it some activation energy ΔE which is independent of the applied stress. The application of an external stress modifies the relative energy of the two states through the addition or subtraction of an additional work term, making a transition in one direction more favorable than its reverse. The strain rate, $\dot{\epsilon}$, may then be written as

$$\dot{\epsilon} = \dot{\epsilon}_o \exp\left(-\frac{\Delta E - \sigma v^*}{kT}\right)$$

where $\dot{\epsilon}_o$ is a prefactor, σ is the applied stress, v^* is the activation volume, k is Boltzmann's constant, and T is the temperature. The activation volume can be determined by the following relation

$$v^* = k\frac{\partial \ln \dot{\epsilon}}{\partial\left(\frac{\sigma}{T}\right)}.$$

Furthermore, this activation volume can be written as the product of the transformation shear strain, $\Delta\epsilon^T$, and the transformation volume, Ω,

$$v^* = \Delta\epsilon^T \Omega.$$

For comparison, experimentally determined activation volumes (for plastic deformation at low strain rate) are

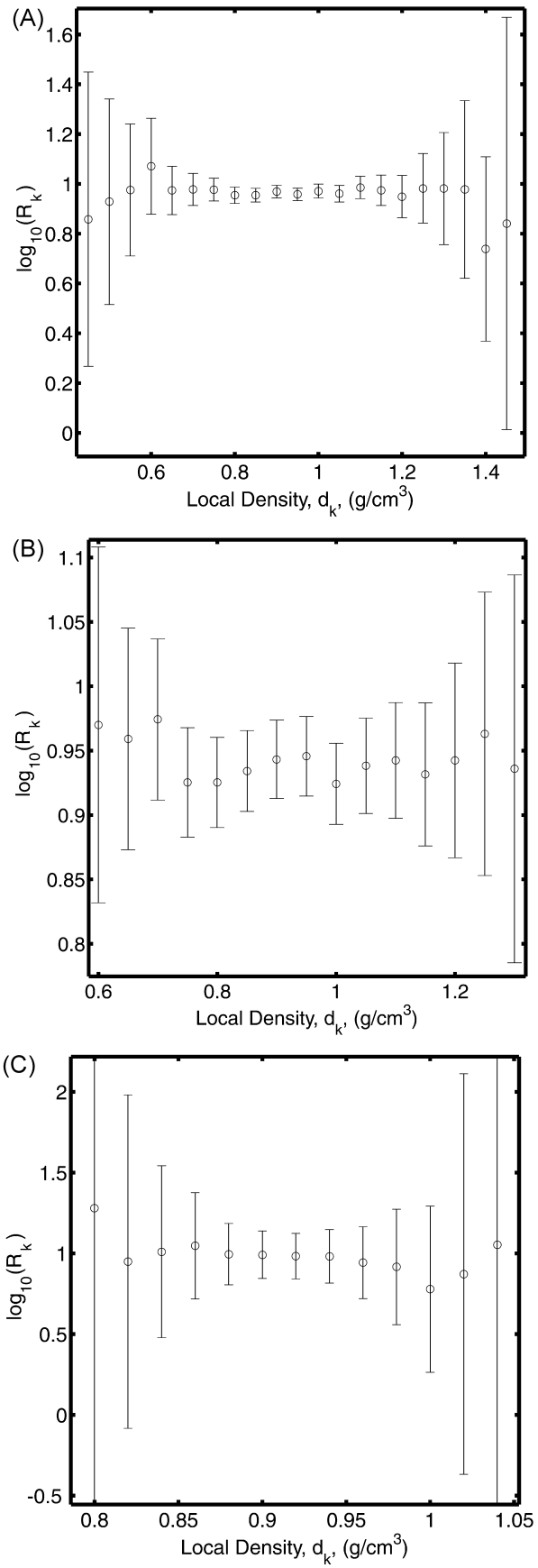

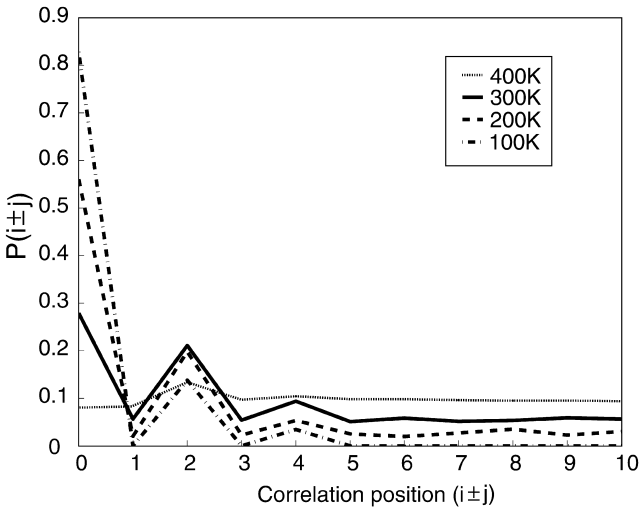

Fig. 10. Neighbor correlation as a function of temperature within non-deforming cells.

found to depend on the particular polymer and range between, for example, 1 nm^3 for PE [43] and 17.2 nm^3 for PET [44].

Fig. 13 displays the yield stress (scaled by temperature) observed during NEMD simulation as a function of strain rate at 100 and 200 K for two different simulation sizes. The yield stress within these simulations was determined by taking the maximum stress that occurs before flow initiates. Results were found to be independent of cell size for cell volumes larger than 109 nm^3, indicating that plastic deformation events occur in a volume much smaller than this. A simultaneous least squares fit to the data at 100 and 200 K for strain rates less than 10^{10} s^{-1} yields an activation volume of $\nu^* = 0.21 \pm 0.03$ nm^3. There is a deviation in the dependence of the yield stress at the higher strain rates. A simultaneous least squares fit to the data at 100 and 200 K for strain rates above 10^{10} s^{-1} results in an activation volume of 0.036 ± 0.002 nm^3. Assuming a transformation strain, $\Delta\epsilon^T$, of 0.017, suggested by quasi-static molecular mechanics calculations on other polymer molecules [4], and an activation volume of 0.21 nm^3, the transformation volume, Ω, is 12.3 nm^3. Assuming the transformation volume is spherical, this leads to a diameter of 2.86 nm, approximately 3.5 times smaller than the simulation cell dimensions (10.1 nm).

Fig. 13 illustrates two distinct regions where linear regression seems to fit the data well. One might imagine that there are various molecular processes which are active at different time scales. Experimentally, it has been observed that a single set of activation parameters may accurately describe polymer yield over some limited range of strain

Fig. 9. The log of the local transition rate per bond per nanosecond, R_k, versus local density in a cell being deformed at a constant true strain rate of 1×10^{10} s^{-1} at 200 K for $\epsilon > 0.3$ and a bin width of (A) 5.21 Å, (B) 6.60 Å, and (C) 17.2 Å.

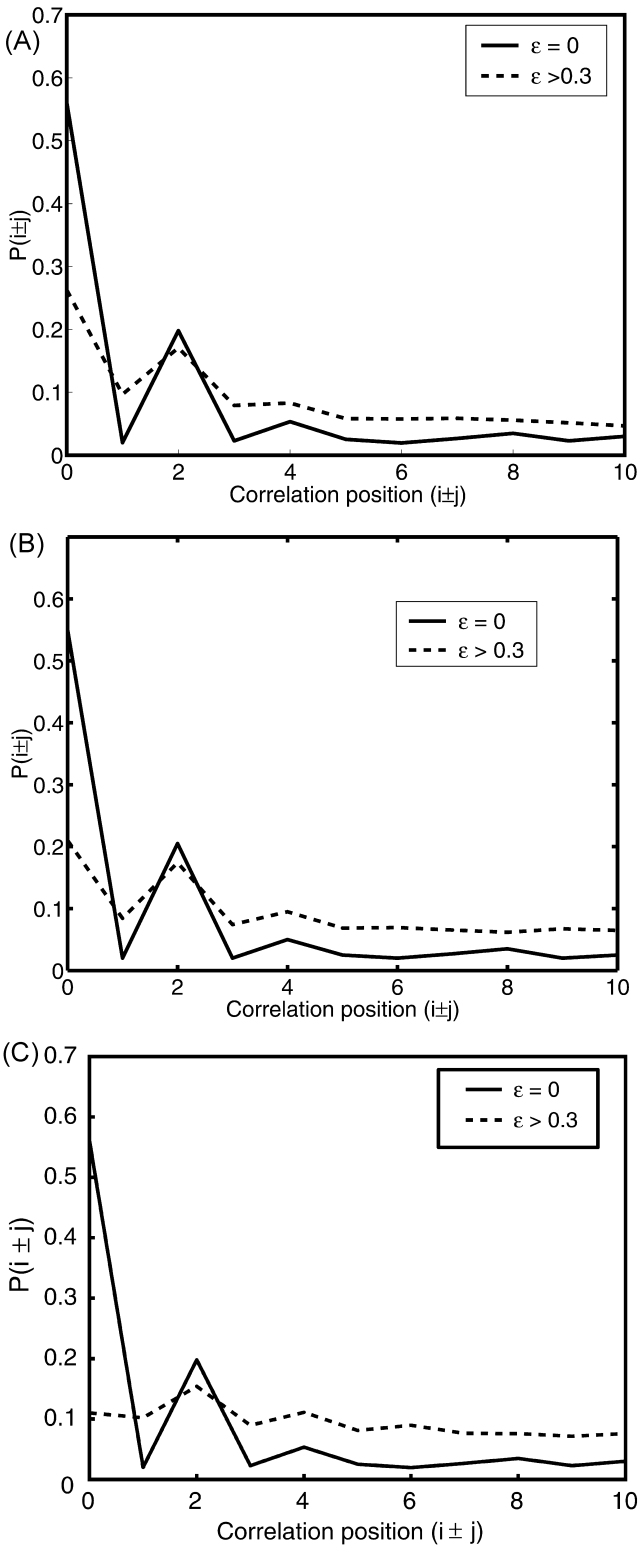

Fig. 11. Neighbor correlation along a chain during deformation at 200 K for a strain rate of (A) $1 \times 10^{10}\,s^{-1}$ in the $NL_x\sigma_y\sigma_zT$ ensemble, (B) $1 \times 10^{10}\,s^{-1}$ deformed at constant volume, and (C) $5 \times 10^{10}\,s^{-1}$ in the $NL_x\sigma_y\sigma_zT$ ensemble.

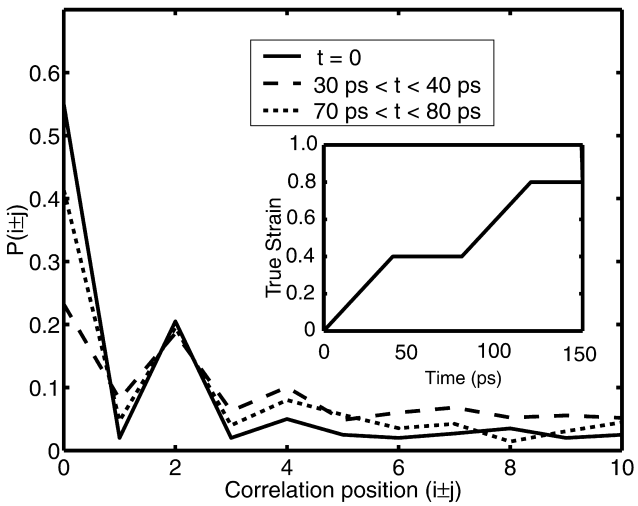

Fig. 12. Comparison of neighbor correlation along a chain during periods of active deformation and relaxation at 200 K with the strain history shown in the inset.

rates, but may fail over more extended regions [45]. Often, the yield stress increases more rapidly at higher strain rates or lower temperatures than it does at lower strain rates or higher temperatures. While there are sub-regions where a single activated process describes the experimental behavior [46], some polymers may require a multiple process Eyring model to produce a good fit over a much wider range of temperatures and strain rates [47,48]. Extrapolating the yield stress in these simulations at 200 K to an experimentally accessible strain rate of 0.01 per second produces an unphysical negative yield stress of −74 MPa. This is a clear indication that additional mechanisms, which would serve to decrease the slope of the yield stress versus logarithm of the strain rate, must be active in flow and relaxation processes during deformations at lower strain rates.

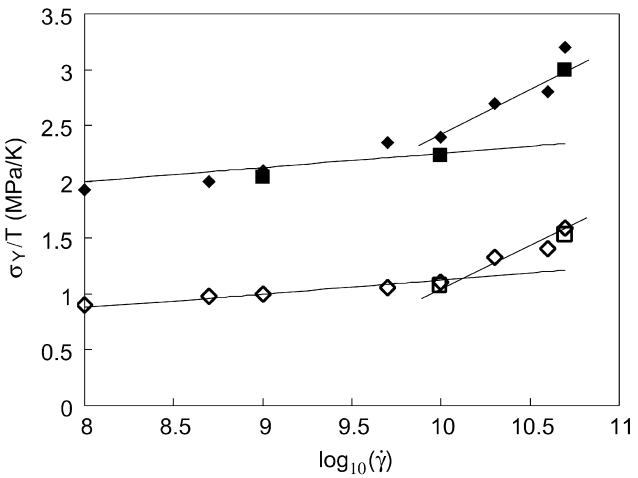

Fig. 13. Yield stress divided by temperature versus the true strain rate for 8000 bead system at 100 K (filled diamonds), 8000 bead system at 200 K (unfilled diamond), 40,000 bead system at 100 K (filled square), 40,000 bead system at 200 K (unfilled squares). Solid lines are the best fit curves.

4. Conclusions

In summary, the simulations reported here reproduce qualitatively the experimentally observed stress–strain behavior of polymer glasses during compressive deformation. In addition, the increased rate of dihedral angle transitions observed with stress within these molecular simulations parallels the stress-induced mobility observed within NMR experiments. Further analysis of the dihedral angle distributions during deformation indicates that this distribution is little changed from the undeformed case until the strain hardening region is obtained, suggesting that a static description of dihedral angle distribution cannot capture the molecular mechanism at yield.

On the other hand, the rate of transition between different states of the dihedral angle distribution is found to increase dramatically during active deformation, and to decrease again as soon as deformation ceases. The intramolecular correlation of such transitions in a chain is also observed to change dramatically during deformation. During active deformation below T_g, this correlation exhibits a form similar to that observed in a non-deforming system above T_g, characterized primarily by fewer self-correlation events. We postulate that the role of active deformation is to permit rearrangement of the molecular structure primarily through enhanced transition dynamics throughout the material. This serves to release pinning points that would otherwise preclude reputation or translation of the chains in response to an applied stress, as well as reduces the probability that subsequent transitions are localized to particular 'active sites'. One might expect furthermore that the transition dynamics are correlated with local variations in density, as suggested by the experimental evidence that associates yield with dilatation. Our simulations show that strain softening following yield occurs when deformation-induced dilation takes place. However, our analyses were unable to detect any correlation between transition dynamics and local density.

Acknowledgements

This work has been supported through NSF Grant No. DMR-98-08941, DURINT Grant No. F49620-01-1-0447, and an NSF graduate fellowship to FMC.

References

[1] Eyring H. J Chem Phys 1936;4:283.
[2] Robertson RE. J Chem Phys 1966;44(10):3950.
[3] Argon AS. Philos Mag 1973;28(4):839–65.
[4] Mott PH, Argon AS, Suter UW. Phys Conden Matter Struct Defects Mech Properties, Philos Mag 1993;67(4):931–78.
[5] Argon AS, Mott PH, Suter UW. Phys Stat Solidi B-Basic Res 1992; 172(1):193–204.
[6] Hutnik M, Argon AS, Suter UW. Macromolecules 1993;26(5): 1097–108.
[7] Malandro DL, Lacks DJ. Comput Theor Polym Sci 1999;9(3-4): 353–7.
[8] Malandro DL, Lacks DJ. J Chem Phys 1999;110(9):4593–601.
[9] Brown D, Clarke JHR. Macromolecules 1991;24(8):2075–82.
[10] Yip S, Sylvester MF, Argon AS. Comput Theor Polym Sci 2000;10(1-2):235–47.
[11] Chui C, Boyce MC. Macromolecules 1999;32(11):3795–808.
[12] Rottler J, Robbins MO. Phys Rev E 2001;6405(5). art. no.-051801.
[13] Loo LS, Cohen RE, Gleason KK. Polymer 2000;41(21):7699–704.
[14] Loo LS, Cohen RE, Gleason KK. Macromolecules 1999;32(13): 4359–64.
[15] Loo LS, Cohen RE, Gleason KK. Science 2000;288(5463):116–9.
[16] Zhou QY, Argon AS, Cohen RE. Polymer 2001;42(2):613–21.
[17] Kim JJ, Choi Y, Suresh S, Argon AS. Science 2002;295(5555): 654–7.
[18] Capaldi FM, Boyce MC, Rutledge GC. Phys Rev Lett 2002;89(17): 175505.
[19] Paul W, Yoon DY, Smith GD. J Chem Phys 1995;103(4):1702–9.
[20] Waheed N, Lavine MS, Rutledge GC. J Chem Phys 2002;116(5): 2301–9.
[21] Verlet L. Phys Rev 1967;159:98.
[22] Berendsen HJC, Postma JPM, van Gunsteren WF, Dinola A, Haak JR. J Chem Phys 1984;81(8):3684–90.
[23] Nose S. J Chem Phys 1984;81(1):511–9.
[24] Hoover WG. Phys Rev A 1985;31(3):1695–7.
[25] Han J, Gee RH, Boyd RH. Macromolecules 1994;27(26):7781–4.
[26] Metropolis N, Rosenbluth A, Rosenbluth M, Tellar A, Tellar M. J Chem Phys 1953;21:1087.
[27] Rigby D, Roe RJ. J Chem Phys 1987;87(12):7285–92.
[28] Yang L, Srolovitz DJ, Yee AF. J Chem Phys 1999;110(14):7058–69.
[29] Takeuchi H, Roe RJ. J Chem Phys 1991;94(11):7458–65.
[30] Gee RH, Boyd RH. Comput Theor Polym Sci 1998;8(1-2):93–8.
[31] Brandrup J, Immergut EH. Polymer handbook, 3rd ed. New York: Wiley-Interscience; 1989.
[32] Hasan OA, Boyce MC, Li XS, Berko S. J Polym Sci Part B-Polym Phys 1993;31(2):185–97.
[33] Hasan OA, Boyce MC. Polymer 1993;34(24):5085–92.
[34] Walley SM, Field JE, Pope PH, Safford NA. J Phys 1991;1(12): 1889–925.
[35] Utz M, Atallah AS, Robyr P, Widmann AH, Ernst RR, Suter UW. Macromolecules 1999;32(19):6191–205.
[36] Khare R, Paulaitis ME. Macromolecules 1995;28(13):4495–504.
[37] Khare R, Paulaitis ME. Chem Engng Sci 1994;49(17):2867–79.
[38] Bharadwaj RK, Boyd RH. J Chem Phys 2001;114(11):5061–8.
[39] Boyd RH, Gee RH, Han J, Jin Y. J Chem Phys 1994;101(1):788–97.
[40] Karatasos K, Adolf DB, Hotston S. J Chem Phys 2000;112(19): 8695–706.
[41] Jin WZ, Boyd RH. Polymer 2002;43(2):503–7.
[42] Jin Y, Boyd RH. J Chem Phys 1998;108(23):9912–23.
[43] Truss RW, Clarke PL, Duckett RA, Ward IM. J Polym Sci Part B-Polym Phys 1984;22:191–209.
[44] Argon AS, Bessonov MI. Philos Mag 1977;35(4):917–33.
[45] Ward IM, Hadley DW. Mechanical properties of solid polymers. West Sussex: Wiley; 1993.
[46] Chen LP, Yee AF, Moskala EJ. Macromolecules 1999;32(18): 5944–55.
[47] Foot JS, Truss RW, Ward IM, Duckett RA. J Mater Sci 1987;22(4): 1437–42.
[48] Bauwens-Crowet C, Bauwens JC, Homes G. J Mater Sci 1972;7:176.